Mode transition in complex refractive index coated single-mode–multimode–single-mode structure

Abian B. Socorro,* Ignacio Del Villar, Jesus M. Corres, Francisco J. Arregui, and Ignacio R. Matias

Electrical and Electronic Engineering Department, Public University of Navarre, Campus Arrosadia s/n, 31006 Pamplona, NA, Spain
**ab.socorro@unavarra.es*

Abstract: By coating a single-mode–multimode–single-mode (SMS) structure with a high refractive index thin-film it is possible to obtain a transition of modes for specific combinations of thin-film thickness, thin-film refractive index and surrounding medium refractive index, which permits to develop devices with a high sensitivity to specific parameters. In order to gain a better knowledge of the phenomenon the experimental results are corroborated numerically with the Transfer-Matrix-Method. The influence of losses in the thin-film has also been studied. The results obtained prove that a thin-film coated SMS structure is a simple and cost-effective platform for development of sensors and optical filters.

OCIS codes: (120.3180) Interferometry; (310.0310) Thin films; (060.2370) Fiber optics sensors.

References and links

1. W. S. Mohammed, P. W. E. Smith, and X. Gu, "All-fiber multimode interference bandpass filter," Opt. Lett. **31**(17), 2547–2549 (2006).
2. J. E. Antonio-Lopez, A. Castillo-Guzman, D. A. May-Arrioja, R. Selvas-Aguilar, and P. Likamwa, "Tunable multimode-interference bandpass fiber filter," Opt. Lett. **35**(3), 324–326 (2010).
3. A. Mehta, W. Mohammed, and E. G. Johnson, "Multimode interference-based fiber-optic displacement sensor," IEEE Photon. Technol. Lett. **15**(8), 1129–1131 (2003).
4. Q. Wu, Y. Semenova, P. Wang, A. M. Hatta, and G. Farrell, "Experimental demonstration of a simple displacement sensor based on a bent single-mode–multimode–single-mode fiber structure," Meas. Sci. Technol. **22**(2), 025203 (2011).
5. Q. Wu, Y. Semenova, A. M. Hatta, P. Wang, and G. Farrell, "Single-mode–multimode–singlemode fiber structures for simultaneous measurement of strain and temperature," Microw. Opt. Technol. Lett. **53**(9), 2181–2185 (2011).
6. V. I. Ruiz-Pérez, M. A. Basurto-Pensado, P. LiKamWa, J. J. Sánchez-Mondragón, and D. A. May-Arrioja, "Fiber optic pressure sensor using multimode interference," J. Phys. Conf. Ser. **274**, 012025 (2011).
7. Q. Wu, Y. Semenova, P. Wang, and G. Farrell, "High sensitivity SMS fiber structure based refractometer--analysis and experiment," Opt. Express **19**(9), 7937–7944 (2011).
8. S. Silva, E. G. P. Pachon, M. A. R. Franco, J. G. Hayashi, F. X. Malcata, O. Frazão, P. Jorge, and C. M. B. Cordeiro, "Ultrahigh-sensitivity temperature fiber sensor based on multimode interference," Appl. Opt. **51**(16), 3236–3242 (2012).
9. L. B. Soldano and E. C. M. Pennings, "Optical multi-mode interference devices based on self-imaging: principles and applications," J. Lightwave Technol. **13**(4), 615–627 (1995).
10. C. R. Biazoli, S. Silva, M. A. R. Franco, O. Frazão, and C. M. B. Cordeiro, "Multimode interference tapered fiber refractive index sensors," Appl. Opt. **51**(24), 5941–5945 (2012).
11. N. D. Rees, S. W. James, R. P. Tatam, and G. J. Ashwell, "Optical fiber long-period gratings with Langmuir-Blodgett thin-film overlays," Opt. Lett. **27**(9), 686–688 (2002).
12. A. B. Socorro, I. Del Villar, J. M. Corres, F. J. Arregui, and I. R. Matias, "Lossy mode resonances dependence on the geometry of a tapered monomode optical fiber," Sens. Actuators A Phys. **180**, 25–31 (2012).
13. I. Del Villar, I. R. Matías, F. J. Arregui, and P. Lalanne, "Optimization of sensitivity in long period fiber gratings with overlay deposition," Opt. Express **13**(1), 56–69 (2005).
14. A. Cusano, A. Iadicicco, P. Pilla, L. Contessa, S. Campopiano, A. Cutolo, and M. Giordano, "Mode transition in high refractive index coated long period gratings," Opt. Express **14**(1), 19–34 (2006).
15. J. M. Corres, I. del Villar, I. R. Matias, and F. J. Arregui, "Fiber-optic pH-sensors in long-period fiber gratings using electrostatic self-assembly," Opt. Lett. **32**(1), 29–31 (2007).

#187483 - $15.00 USD Received 20 Mar 2013; revised 3 May 2013; accepted 13 May 2013; published 16 May 2013

16. Z. Gu, Y. Xu, and K. Gao, "Optical fiber long-period grating with solgel coating for gas sensor," Opt. Lett. **31**(16), 2405–2407 (2006).
17. C. R. Zamarreño, M. Hernáez, I. Del Villar, I. R. Matías, and F. J. Arregui, "Optical fiber pH sensor based on lossy-mode resonances by means of thin polymeric coatings," Sens. Actuators B Chem. **155**(1), 290–297 (2011).
18. P. Pilla, A. Iadicicco, L. Contessa, S. Campopiano, A. Cutolo, M. Giordano, and A. Cusano, "Optical chemo-sensor based on long period fiber gratings coated with d form syndiotactic polystyrene," IEEE Photon. Technol. Lett. **17**(8), 1713–1715 (2005).
19. D. W. Kim, Y. Zhang, K. L. Cooper, and A. Wang, "Fibre-optic interferometric immuno-sensor using long period grating," Electron. Lett. **42**(6), 324–325 (2006).
20. L. L. Xue and L. Yang, "Sensitivity enhancement of RI sensor based on SMS fiber structure with high refractive index overlay," J. Lightwave Technol. **30**(10), 1463–1469 (2012).
21. G. W. Chern and L. A. Wang, "Transfer matrix method based on perturbation expansion for periodic and quasi-periodic binary long-period fiber gratings," J. Opt. Soc. Am. A **16**(11), 2675–2689 (1999).
22. P. Yeh, A. Yariv, and E. Marom, "Theory of Bragg fiber," J. Opt. Soc. Am. **68**(9), 1196–1201 (1978).
23. T. Erdogan, "Cladding-mode resonances in short and long period fiber gratings filters," J. Opt. Soc. Am. A **14**(8), 1760–1773 (1997).
24. G. Decher, "Fuzzy nanoassemblies: toward layered polymeric multicomposites," Science **277**(5330), 1232–1237 (1997).
25. I. Del Villar, I. R. Matias, F. J. Arregui, and M. Achaerandio, "Nanodeposition of materials with complex refractive index in long-period fiber gratings," J. Lightwave Technol. **23**(12), 4192–4199 (2005).
26. I. Del Villar, I. R. Matias, F. J. Arregui, and R. O. Claus, "Fiber-optic hydrogen peroxide nanosensor," IEEE Sens. J. **5**(3), 365–371 (2005).

1. Introduction

Single-mode–multimode–single-mode (SMS) fiber is used in important fields such as optical communications and sensors. In optical communications interesting devices such as wavelength filters have been developed [1,2], whereas in optical sensors field it has been possible to measure magnitudes such as displacement, strain, pressure, temperature or refractive index [2–8].

The basic physical principle of the device is that light transmitted through the fundamental mode of the SMF segment is coupled to several modes into the MMF section and recoupled to the fundamental mode of the SMF at the end of the MMF segment [8]. Due to the phenomenon of multimodal interferometry (MMI) both transmission and attenuation bands are obtained in the optical spectrum. Particularly, the transmission bands obtained by the self-imaging effect exhibit minimum losses [9], and its central wavelength can be controlled as a function of the MMF segment dimensions, mainly the MMF segment length and diameter [8].

The MMF segment diameter is also responsible for the sensitivity of the device. In [7,8] it has been proved that, by reducing the diameter, an improved sensitivity to refractive index can be obtained. However, there are additional problems such as fiber misalignment and adequate splicing to the SMF fiber. That is why in [10] it has been proposed a tapered SMS.

Additionally there is also an increasing interest in developing structures coated with thin films [11–19].

Two reasons justify the application of an additional coating. The first one is the ability to improve the performance of the same devices without coating [13]. As an example it has been possible to obtain a 10 fold increase in long-period fiber grating refractometers [14]. The second reason is the possibility to use coatings that are sensitive to humidity [15], a specific gas [16], pH [17], a chemical species [18], or a biological species [19], which permits to increase the number of applications of these devices in a great manner.

In view of the previous success in combining thin-films with optical structures that are inherently sensitive to the surrounding medium, the application of a thin-film to an SMS structure should lead to interesting results. So far this idea has been studied theoretically in [20], showing promising results such as the improvement, as a function of coating thickness, of the sensitivity of one of the resonances created in the optical spectrum.

In this work the previous question is proved experimentally for the first time to our knowledge. In addition to this, simulation data obtained with the transfer-matrix-method permit to understand the influence of losses in the thin-film in terms of visibility of the intereferences obtained in the optical spectrum. The phenomenon owns similarities with thin-film coated LPFGs, where there is a progressive blue wavelength shift of the resonances as a

#187483 - $15.00 USD Received 20 Mar 2013; revised 3 May 2013; accepted 13 May 2013; published 16 May 2013

function of the coating thickness [21]. The phenomenon is caused by a modification of the effective index of cladding modes induced by the thin-film, which in some works is called "mode transition" [13,14]. In the SMS there is also a wavelength shift caused by the modification of the effective index of cladding modes. Contrary to LPFGs there is a wavelength shift to the red, which will be explained later. In addition to this, the results obtained for different MMF section lengths permit to obtain important conclusions that can be applied for the miniaturization of these devices.

In section 2 a simulation method for the analysis of SMS structures is explained. In section 3 the experimental procedure is detailed. Numerical and experimental data are presented and discussed in section 4. Finally, some conclusions are included in section 5.

2. Theory

In order to obtain the optical transmission through the SMS structure, a simulation tool is developed based on the transfer matrix method [22]. The procedure for obtaining the transmission as a function of wavelength is based on three steps:

2.1 Calculation of the propagation constants

The application of the transfer matrix method presented in [23], permits to calculate the propagation constants of modes in a cylindrical waveguide by expressing their fields in terms of radial and azimuthal vector components. In the SMS structure of Fig. 1 there are two different waveguides, whose propagation constants are calculated. In view of the azimuthal symmetry of the waveguides, only modes with azimuthal order ν = 1 are considered for the analysis [24]. Consequently, the notation for modes will be of the type '1,j' (the first subindex representing the azimuthal order, and the second subindex indicating the j^{th} mode).

2.2 Derivation of the transmission and reflection coefficients

Considering in Fig. 1 the SMF on the left side of the SMS structure as waveguide 'a', the coreless MMF as waveguide 'b', and the SMF on the right side as waveguide 'c', the transmission and reflection coefficients can be obtained with this general equation:

$$\begin{pmatrix} A_{11}^{(c)} \\ B_{11}^{(c)} \\ A_{12}^{(c)} \\ B_{12}^{(c)} \\ \vdots \\ A_{1N}^{(c)} \\ B_{1N}^{(c)} \end{pmatrix} = H_{cb} \cdot F \cdot H_{ba} \begin{pmatrix} A_{11}^{(a)} \\ B_{11}^{(a)} \\ A_{12}^{(a)} \\ B_{12}^{(a)} \\ \vdots \\ A_{1N}^{(a)} \\ B_{1N}^{(a)} \end{pmatrix} \quad (1)$$

where $A_{1j}(a)$ is the normalized forward amplitude of the j mode in waveguide 'a', $A_{1j}(c)$ is the normalized forward amplitude of the j mode in waveguide 'c', $B_{1j}(a)$ is the normalized backward amplitude of the j mode in waveguide 'a', and $B_{1j}(c)$ is the normalized backward amplitude of the j mode in waveguide 'c'.

H_{ba} and H_{cb} are the matrices that relate the amplitudes of the modes at both sides of the interface between waveguide 'b' and 'a', and between waveguide 'c' and 'b' respectively. As an example of both expressions, according to [22], matrix H_{cb}, which relates the amplitude of the modes at both sides of the interface between waveguide c and b, can be expressed as indicated in Eq. (2):

#187483 - $15.00 USD Received 20 Mar 2013; revised 3 May 2013; accepted 13 May 2013; published 16 May 2013

$$\begin{pmatrix} A_{11}^{(c)} \\ B_{11}^{(c)} \\ A_{12}^{(c)} \\ B_{12}^{(c)} \\ \vdots \\ A_{0N}^{(c)} \\ B_{1N}^{(c)} \end{pmatrix} = \begin{pmatrix} \frac{1}{2}\left(I_{11,11}+J_{11,11}\right) & \frac{1}{2}\left(I_{11,11}-J_{11,11}\right) & \frac{1}{2}\left(I_{11,12}+J_{11,12}\right) & \frac{1}{2}\left(I_{11,12}-J_{11,12}\right) & \cdots & \frac{1}{2}\left(I_{11,1N}+J_{11,1N}\right) & \frac{1}{2}\left(I_{11,1N}-J_{11,1N}\right) \\ \frac{1}{2}\left(I_{11,11}-J_{11,11}\right) & \frac{1}{2}\left(I_{11,11}+J_{11,11}\right) & \frac{1}{2}\left(I_{11,12}-J_{11,12}\right) & \frac{1}{2}\left(I_{11,12}+J_{11,12}\right) & \cdots & \frac{1}{2}\left(I_{11,1N}+J_{11,1N}\right) & \frac{1}{2}\left(I_{11,1N}+J_{11,1N}\right) \\ \frac{1}{2}\left(I_{12,11}+J_{12,11}\right) & \frac{1}{2}\left(I_{12,11}-J_{12,11}\right) & \frac{1}{2}\left(I_{12,12}+J_{12,12}\right) & \frac{1}{2}\left(I_{12,12}-J_{12,12}\right) & \cdots & \frac{1}{2}\left(I_{12,1N}+J_{12,1N}\right) & \frac{1}{2}\left(I_{12,1N}+J_{12,1N}\right) \\ \frac{1}{2}\left(I_{12,11}-J_{12,11}\right) & \frac{1}{2}\left(I_{12,11}+J_{12,11}\right) & \frac{1}{2}\left(I_{12,12}-J_{12,12}\right) & \frac{1}{2}\left(I_{12,12}+J_{12,12}\right) & \cdots & \frac{1}{2}\left(I_{12,1N}+J_{12,1N}\right) & \frac{1}{2}\left(I_{12,1N}+J_{12,1N}\right) \\ \vdots & \vdots & \vdots & \vdots & \ddots & \vdots & \vdots \\ \frac{1}{2}\left(I_{1N,11}+J_{1N,11}\right) & \frac{1}{2}\left(I_{1N,11}-J_{1N,11}\right) & \frac{1}{2}\left(I_{1N,12}+J_{1N,12}\right) & \frac{1}{2}\left(I_{1N,12}-J_{1N,12}\right) & \cdots & \frac{1}{2}\left(I_{1N,1N}+J_{1N,1N}\right) & \frac{1}{2}\left(I_{1N,1N}+J_{1N,1N}\right) \\ \frac{1}{2}\left(I_{1N,11}-J_{1N,11}\right) & \frac{1}{2}\left(I_{1N,11}+J_{1N,11}\right) & \frac{1}{2}\left(I_{1N,12}-J_{1N,12}\right) & \frac{1}{2}\left(I_{1N,12}+J_{1N,12}\right) & \cdots & \frac{1}{2}\left(I_{1N,1N}+J_{1N,1N}\right) & \frac{1}{2}\left(I_{1N,1N}+J_{1N,1N}\right) \end{pmatrix} \begin{pmatrix} A_{11}^{(b)} \\ B_{11}^{(b)} \\ A_{12}^{(b)} \\ B_{12}^{(b)} \\ \vdots \\ A_{1N}^{(b)} \\ A_{1N}^{(b)} \end{pmatrix} \quad (2)$$

where $I_{1j,1k}$ and $J_{1j,1k}$ are the following expressions:

$$I_{1k,1j} = \sqrt{P_{1j}^{-1}P_{1k}^{-1}}\frac{1}{2}\mathrm{Re}\int_{\phi=0}^{2\pi}d\phi\int_{r=0}^{\infty}\left[E_{1,j-r}^{b}(r)H_{1,k-\phi}^{a}(r)^{*} - H_{1,k-r}^{a}(r)^{*}E_{1,j-\phi}^{b}(r)\right]rdr \quad (3)$$

$$J_{1k,1j} = \sqrt{P_{1j}^{-1}P_{1k}^{-1}}\frac{1}{2}\mathrm{Re}\int_{\phi=0}^{2\pi}d\phi\int_{r=0}^{\infty}\left[E_{1,j-r}^{a}(r)^{*}H_{1,k-\phi}^{b}(r) - H_{1,k-r}^{b}(r)E_{1,j-\phi}^{a}(r)^{*}\right]rdr \quad (4)$$

In expressions (3) and (4) $E_{1,j\text{-}r}$ is the radial electric field of $mode_{1,j}$, $E_{1,j\text{-}\phi}$ is the azimuthal electric field of $mode_{1,j}$, $H_{1,j\text{-}r}$ is the radial magnetic field of $mode_{1,j}$, $H_{1,j\text{-}\phi}$ is the azimuthal magnetic field of $mode_{1,j}$, and $P_{1,j}$ is the normalized power of the same mode.

The expression for matrix F, which is the free propagation matrix over the MMF region of length L is:

$$F = \begin{pmatrix} \exp(-j\beta_{11}L) & 0 & 0 & 0 & \cdots & 0 & 0 \\ 0 & \exp(j\beta_{11}L) & 0 & 0 & \cdots & 0 & 0 \\ 0 & 0 & \exp(-j\beta_{12}L) & 0 & \cdots & 0 & 0 \\ 0 & 0 & 0 & \exp(j\beta_{12}L) & \cdots & 0 & 0 \\ \vdots & \vdots & \vdots & \vdots & \ddots & \vdots & \vdots \\ 0 & 0 & 0 & 0 & \cdots & \exp(-j\beta_{1N}L) & 0 \\ 0 & 0 & 0 & 0 & \cdots & 0 & \exp(j\beta_{1N}L) \end{pmatrix} \quad (5)$$

where β_{1j} is the propagation constant of $mode_{1,j}$.

2.2 Derivation of the transmission and reflection coefficients

The transmission can be found by assuming in expression (1) that only one mode is incident ($A(a)_{1,1} = 1$ and $A(a)_{1,2} = \ldots.. = A(a)_{1,N} = 0$) and that there is no backward reflection in waveguide 'c' ($B(c)_{1,1} = B(c)_{1,2} = \ldots.. = B(c)_{1,N} = 0$), and solving the equation. After that, the transmission power can be expressed as:

$$T = \left|A_{11}^{c}\right|^{2} \quad (6)$$

3. Experimental section

The SMS structure is fabricated by splicing a segment of coreless multimode fiber (MMF) from POFC Inc. to two standard SMF pigtails from Telnet Inc (see Fig. 1). The diameter of all fibers is 125 μm.

#187483 - $15.00 USD Received 20 Mar 2013; revised 3 May 2013; accepted 13 May 2013; published 16 May 2013

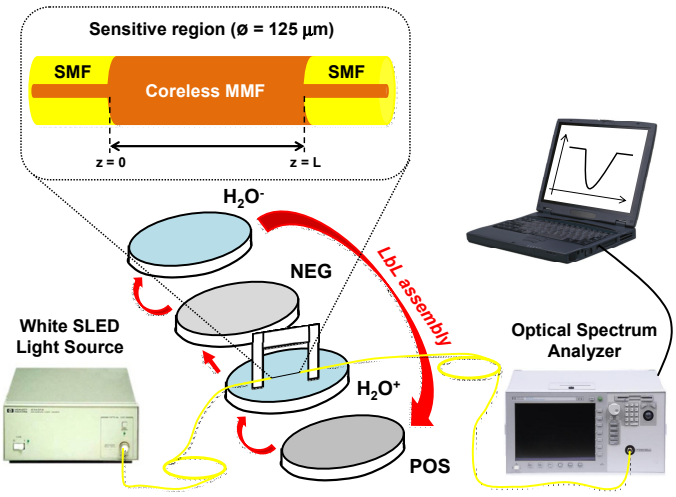

Fig. 1. Experimental setup.

Devices with different MMF section length are developed with lengths 5, 10, 15, 20, 25, 30, 35, 40, 45, 50 and 58 mm respectively.

For the deposition of the thin-film, layer-by-layer self-assembly process (LbL) is used [25]. Each bilayer of the coating is obtained by immersing the substrate in two solutions of poly (allylamine hydrochloride) (PAH) and poly (acrylic acid) (PAA), both of them in 10 mM concentration and adjusted to pH 4.5. These polymers were purchased from Sigma-Aldrich [18].

At one side, a super luminescent emitting diode light source (HP_83437A – SLED from Agilent Inc.) launches light in a wavelength range between 1150 and 1680 nm into the SMS structure. At the other side, the light modulated by the SMS is detected by a HP-86142A optical spectrum analyzer (OSA) from Agilent Inc.

4. Results

As it was indicated in the experimental section, SMS structures with different MMF section length were fabricated; from 5 to 58 mm. In Fig. 2 it can be observed the good agreement between theoretical and experimental data. Different transmission and attenuation bands can be observed in the optical spectrum of all devices.

#187483 - $15.00 USD Received 20 Mar 2013; revised 3 May 2013; accepted 13 May 2013; published 16 May 2013

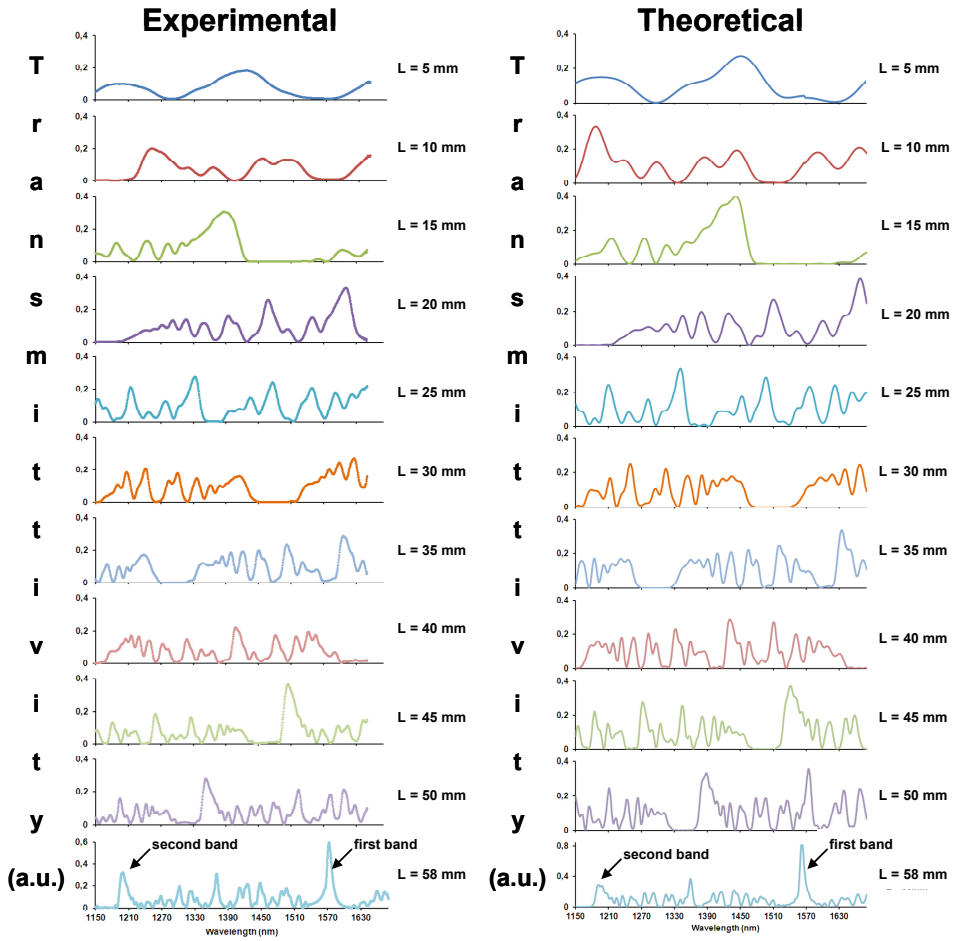

Fig. 2. Experimental and theoretical spectra of uncoated SMS structure for different MMF section lengths: 5, 10, 15, 20, 25, 30, 35, 40, 45, 50 and 58 mm.

These bands are caused by multimodal interferometry, which can be constructive or destructive. If interferometry is constructive it may be caused by a fractional constructive interference or by a light field condensation between the several guided modes in a particular plane (the self-imaging effect) [10]. The last option permits to obtain a higher transmission than in the rest of cases. Consequently, the next design has been focused on monitoring the evolution of the band produced by the self-imaging effect. In this sense, the design can be simplified in a great manner by using the analytical expression that approximates the length of the MMF section that is adequate for positioning the band at a specific wavelength [10]:

$$Z_i = \frac{4D^2 n}{\lambda} \tag{7}$$

where D and n are the MMF diameter and refractive index, respectively, and λ is the operational wavelength.

According to the experimental section D is 125 μm. Consequently, just by fixing the refractive index and the operational wavelength, the length of MMF segment can be determined. In view of the wavelength range that is monitored with the experimental setup of Fig. 1, a good option is to fix the transmission band at the third optical communications

#187483 - $15.00 USD Received 20 Mar 2013; revised 3 May 2013; accepted 13 May 2013; published 16 May 2013

window: 1550 nm. At this wavelength the refractive index of silica is 1.444, which can be applied to variable *n*. So the length of the MMF segment should be 58 mm.

The last plot represented in Fig. 2 confirms this fact. The transmission band observed at the third optical communications window is the one with the highest transmission. Moreover, the good approximation of expression (7) is proved both experimentally and numerically with the method explained in section 2.

After seeing that the most important band belongs to the 58 mm device, it will be used as the substrate to deposit progressively a thin-film by means of the LbL method. According to the indications of section 3, the optical spectrum is represented in Fig. 3 as a function of the number of bilayers of PAH/PAA. A wavelength shift to the red is observed for all bands, which indicates that expression (7) is no longer valid if a thin-film is deposited on the MMF section.

If we compare the experimental results with numerical data (see Fig. 4) obtained with the method explained in section 2, it is easy to observe the similarity in the evolution of the transmission bands. However, there is an important difference in terms of fading of the transmission bands. In the region between 450 and 650 nm the experimental data show a null transmission, a phenomenon that has been observed in thin-film coated long-period fiber gratings (LPFGs) [11,26], in thin-film coated cladding removed multimode optical fibers [17] and in thin-film coated tapered fibers [12]. This phenomenon is caused by coupling of light to a mode guided in a thin-film that presents losses and it is not considered in Fig. 4. According to our estimations [26], the refractive index of PAH/PAA at 1310 nm was 1.5 + 0.0025i. The real part of this value was used for obtaining the numerical results of Fig. 4. However, if the complex refractive index is considered, the theoretical results obtained in Fig. 5 fit better with those of Fig. 3.

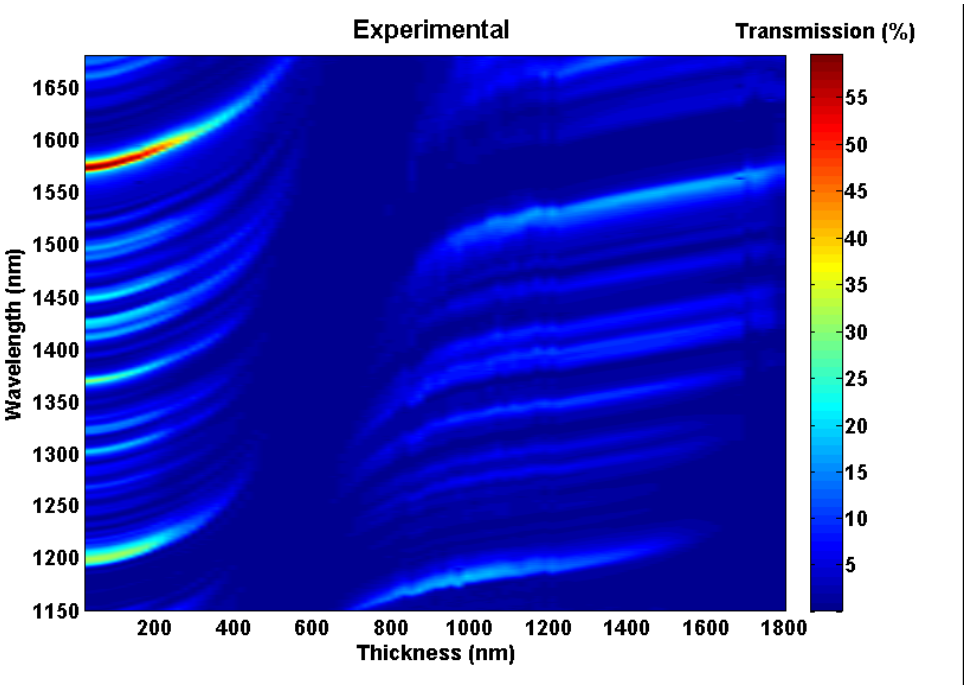

Fig. 3. Evolution of the spectrum as a function of thickness for an SMS structure of 58 mm (experimental results).

#187483 - $15.00 USD Received 20 Mar 2013; revised 3 May 2013; accepted 13 May 2013; published 16 May 2013

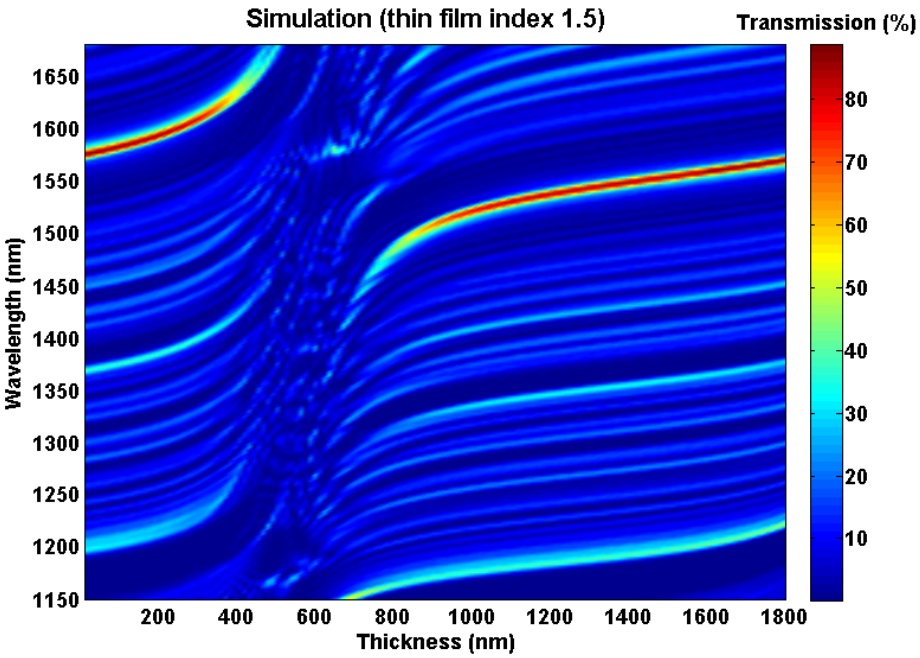

Fig. 4. Evolution of the spectrum as a function of thickness for an SMS structure of 58 mm (simulation with thin-film refractive index 1.5).

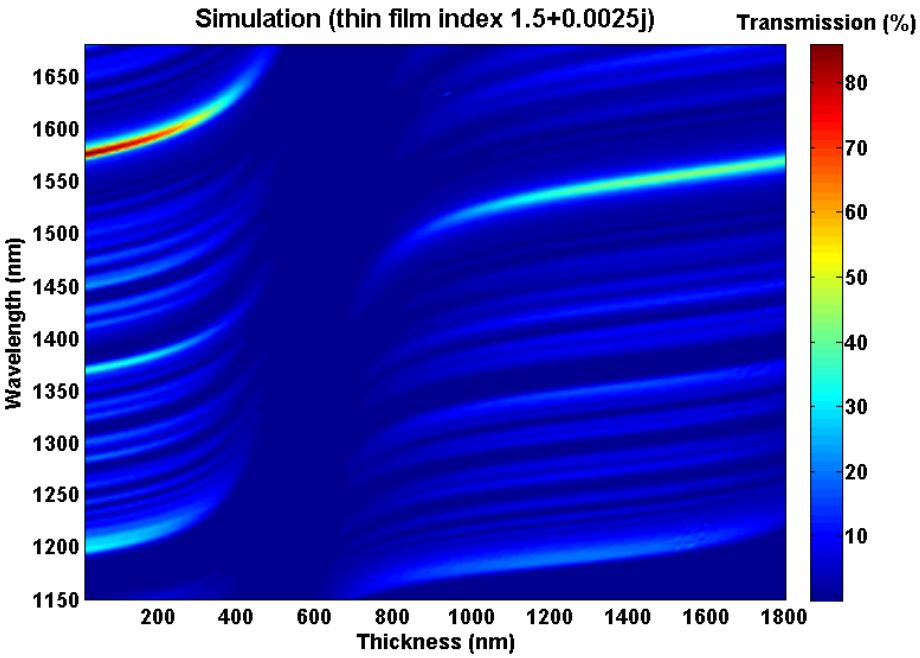

Fig. 5. Evolution of the spectrum as a function of thickness for an SMS structure of 58 mm (simulation with thin-film refractive index 1.5 + 0.0025i).

#187483 - $15.00 USD Received 20 Mar 2013; revised 3 May 2013; accepted 13 May 2013; published 16 May 2013

In Fig. 6, the central wavelength of the transmission bands and its maximum power is represented both theoretically and experimentally, confirming the similarity between the model and the experimental data.

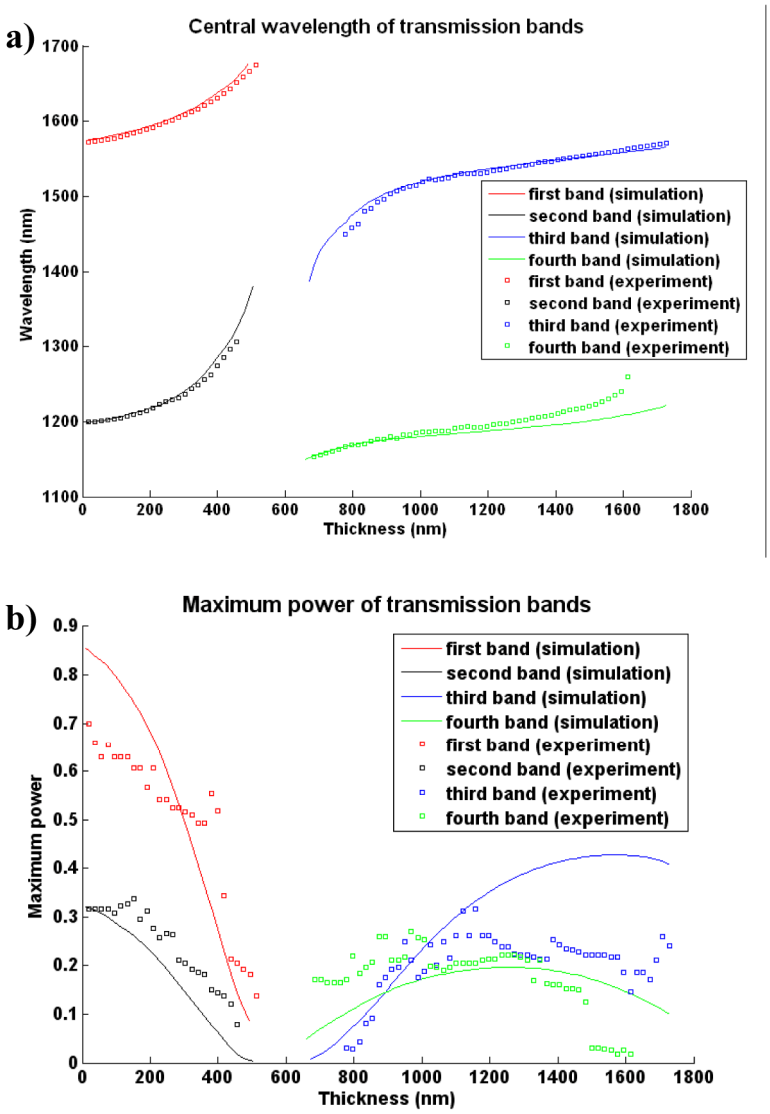

Fig. 6. Evolution as a function of thickness of a) the central wavelength of two transmission bands obtained with an SMS structure of 58 mm b) the maximum power of two transmission bands obtained with an SMS structure of 58 mm.

It can be observed in the plots that, after the fading region, the transmission bands recover but with an additional attenuation. Consequently, for an application in sensing or communications domain, the region between 0 and 450 nm is the best option. Moreover, the wavelength shift rate increases as a function of the thin-film thickness, confirming the analysis of [20]. This conclusion can be used for the design of optimized optical fiber sensors.

It is also interesting to observe the shape of plots in Figs. 3, 4, 5 and 6. It resembles to those plots obtained with deposition of thin-films on LPFGs [13,14]. However, instead of a blue wavelength shift, transmission bands experiment a wavelength shift to the red.

#187483 - $15.00 USD Received 20 Mar 2013; revised 3 May 2013; accepted 13 May 2013; published 16 May 2013

If we consider in Fig. 7 the evolution of the effective index of modes in the MMF segment, it is easy to observe that in the fading region there is a double step mode transition (the $HE_{1,7}$ mode becomes de $HE_{1,5}$ mode, the $EH_{1,6}$ becomes the $EH_{1,4}$, and so on), exactly like cladding modes in LPFGs [21].

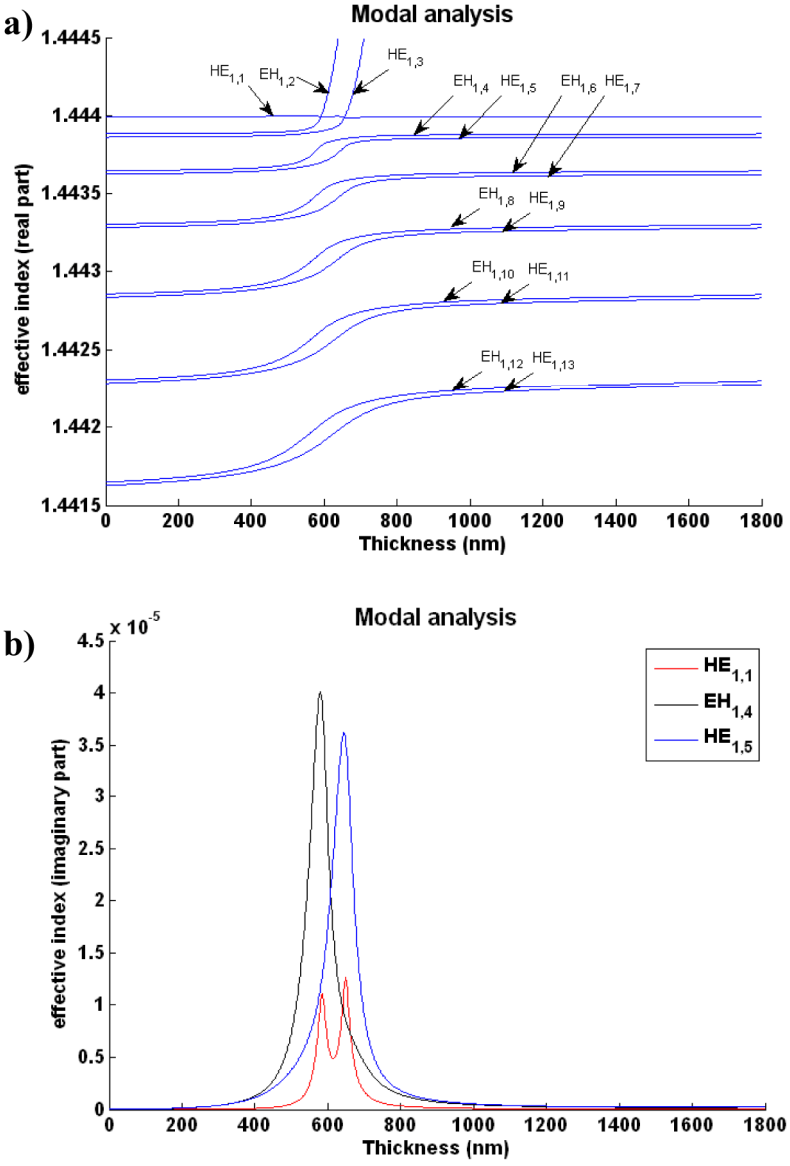

Fig. 7. Evolution as a function of thickness of the effective index of modes in the MMF section of an SMS structure (incidence wavelength 1550 nm).

In LPFGs each resonance is caused by coupling of light from the core mode to a cladding mode. Attenuation bands caused by coupling to cladding modes of higher order are located at higher wavelengths whereas the opposite is true for bands induced by coupling to lower order modes. Consequently, the same transition of the effective indices of cladding modes is observed for the attenuation bands (the band of the $HE_{1,7}$ mode experiments a blue shift to the band of the $HE_{1,5}$ mode, the band of the $EH_{1,6}$ experiments a blue shift to the band of the $EH_{1,4}$ mode and so on) [13].

#187483 - $15.00 USD Received 20 Mar 2013; revised 3 May 2013; accepted 13 May 2013; published 16 May 2013

In an SMS structure there is also a transition of modes (see Fig. 7(a)). Unlike in LPFGs, attenuation and transmission bands are produced by constructive and destructive interference among several modes. Focusing on constructive interference, this phenomenon occurs if the difference between the phases of modes is a multiple of 2π. The phase is directly proportional to the separation between the effective indices of the modes guided in the MMF section and to the length of the MMF section, and inversely proportional to the incident wavelength. By considering Fig. 7(a), higher order modes experiment a higher effective index increase than lower order modes. In addition to this, the phase of higher order modes exceeds that of lower order modes. Consequently, the phase difference between the modes is increased. In view of the fact that the difference in phase is inversely proportional to the incidence wavelength, this last parameter must be increased in order to continue satisfying the condition for constructive interference. In other words, there is a wavelength shift to the red, which also occurs for bands with destructive interference, following the same explanation but for a phase difference of an uneven multiple of π.

If we analyze in Fig. 8 the constructive interference points between $HE_{1,1}$ and $HE_{1,3}$ modes in the MMF segment, it is easy to visualize the two main bands of Figs. 3, 4 and 5. They experiment a wavelength shift to the red because $HE_{1,1}$ increases more slowly as a function of the thin-film thickness than $HE_{1,3}$ (see Fig. 7(a)).

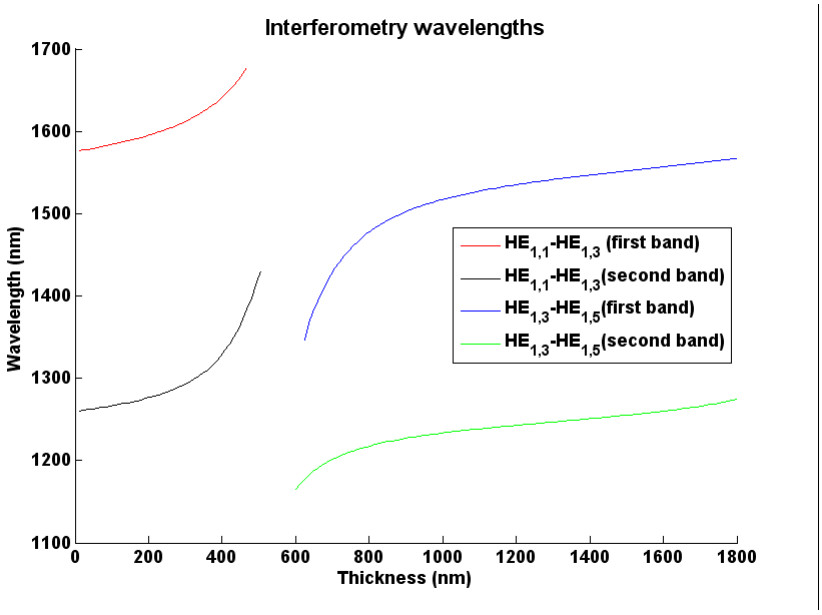

Fig. 8. Evolution as a function of thickness of the constructive interference wavelengths of mode $HE_{1,1}$ and $HE_{1,3}$ in the MMF section of and SMS structure.

The reason why the constructive interference between the two first even modes coincides exactly with the main bands can be understood in Fig. 9, where the normalized coupling factor between the fundamental mode guided in the core of the SMF section and the modes guided in the MMF section is plotted. Out of the fading region observed in Fig. 4 there is a maximum coupling to uneven modes. Consequently, interference among uneven modes is the predominant. Since among the group of uneven modes, $HE_{1,1}$ and $HE_{1,3}$ are the ones with a lowest separation in effective index, the wavelengths where constructive interference occurs are more separated than for the rest of modes.

#187483 - $15.00 USD Received 20 Mar 2013; revised 3 May 2013; accepted 13 May 2013; published 16 May 2013

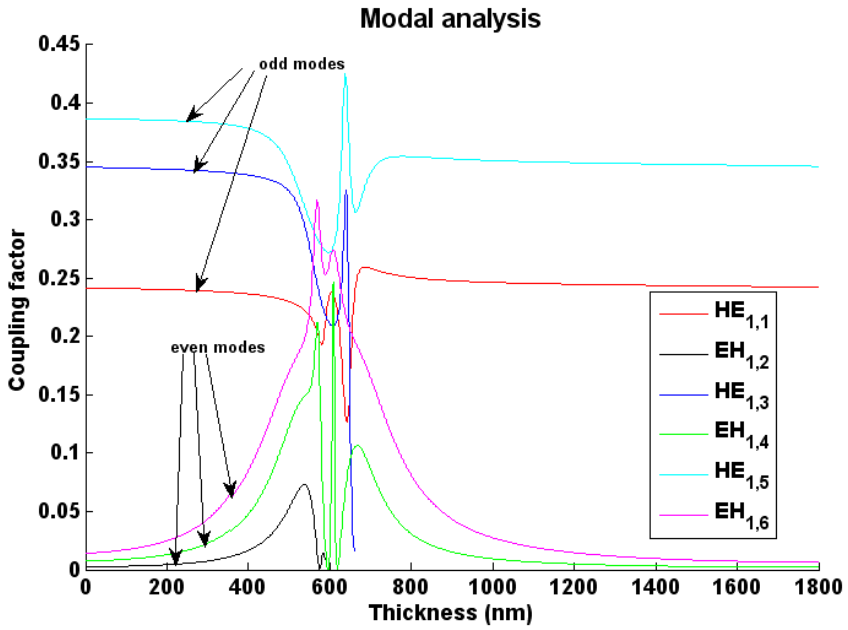

Fig. 9. Evolution as a function of thickness of the coupling between the fundamental mode of the SMF section and the modes in the MMF section in an SMS structure (incidence wavelength 1550 nm).

However, it is obvious that each band may obey to constructive interference among several modes. In fact the band located at the third optical communications window is where the self-imaging effect occurs. Consequently, it is obvious that there are other constructive interferences concurrent at that position. In this sense, the uniform evolution of the transmission bands indicates that the evolution of the difference between the effective indices of all modes is proportional. The increase in the effective index of $HE_{1,1}$ is lower than that of $HE_{1,3}$ and the increase of $HE_{1,3}$ is lower that that of HE_{15}, and so on. Only in the transition region the original bands disappear and new ones are created if the thin-film presents no losses (see Fig. 4). This is due to the abrupt change in the coupling conditions between the fundamental mode of the SMF section and the modes in the MMF section as it can be observed in Fig. 9.

However, if the thin-film presents losses there is an increase in the imaginary part of the effective index of modes (see Fig. 7(b)), which causes a reduction of the optical transmission (see Fig. 5), something that occurred also for LPFGs.

Another important conclusion can be extracted from Fig. 6(a). The two bands plotted from 0 to 450 nm experiment the same wavelength shift with the exception of a factor depending on the wavelength. Consequently, many bands can be monitored at the same time, which should increase the accuracy of the device if it is used for sensing purposes. Moreover, if devices with different MMF section length are designed and transmission bands are centered at the same wavelength, they experiment the same wavelength shift, which has consequences in terms of miniaturization of the SMS structure. This idea is proved by analyzing an SMS structure of 20 mm, with and initial spectrum represented in Fig. 2. Even though it is obvious that the shape of the spectrum is different to that of the 58 mm SMS, in Fig. 10 it can be visualized that the initial spectrum of Fig. 2 experiments a similar wavelength shift to that observed in Fig. 4. The results of Fig. 10 are contrasted with the numerical data obtained for a thin-film with and without losses (see Figs. 11 and 12). Like in the 58 mm SMS device, the second option agrees better with the experimental results.

#187483 - $15.00 USD Received 20 Mar 2013; revised 3 May 2013; accepted 13 May 2013; published 16 May 2013

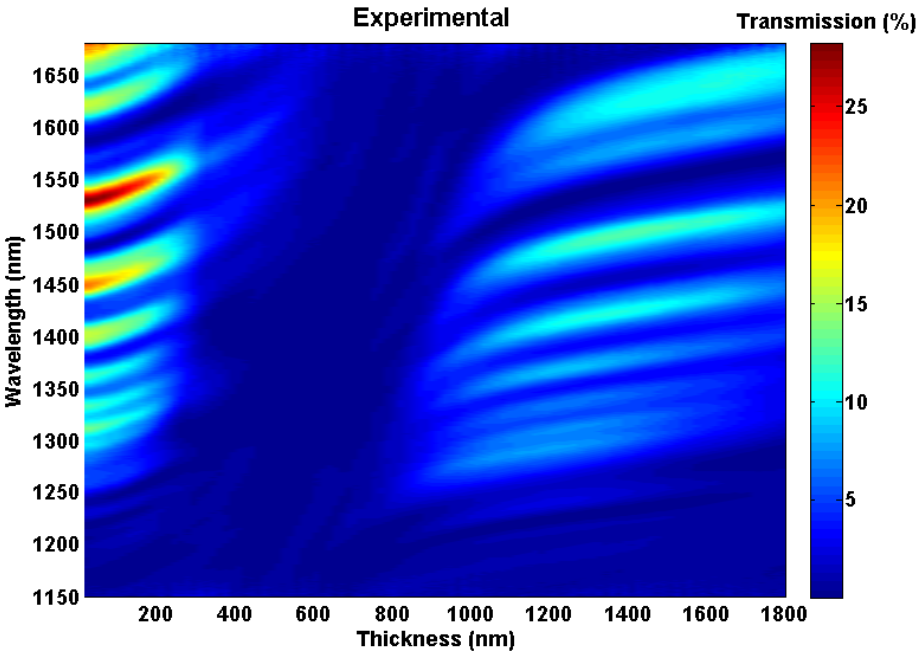

Fig. 10. Evolution of the spectrum as a function of thickness for an SMS structure of 20 mm (experimental results).

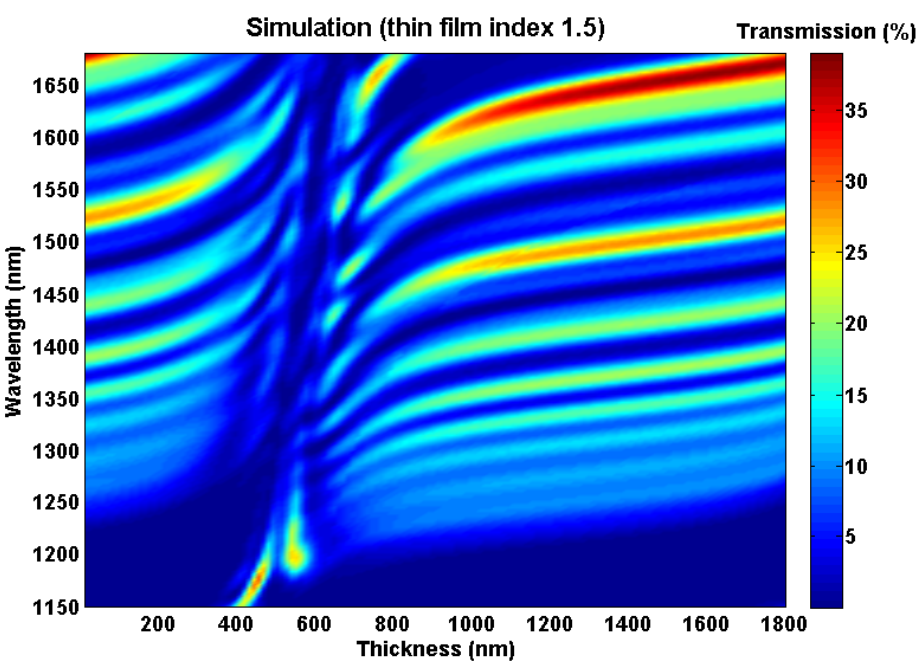

Fig. 11. Evolution of the spectrum as a function of thickness for an SMS structure of 20 mm (simulation with thin-film refractive index 1.5).

#187483 - $15.00 USD Received 20 Mar 2013; revised 3 May 2013; accepted 13 May 2013; published 16 May 2013

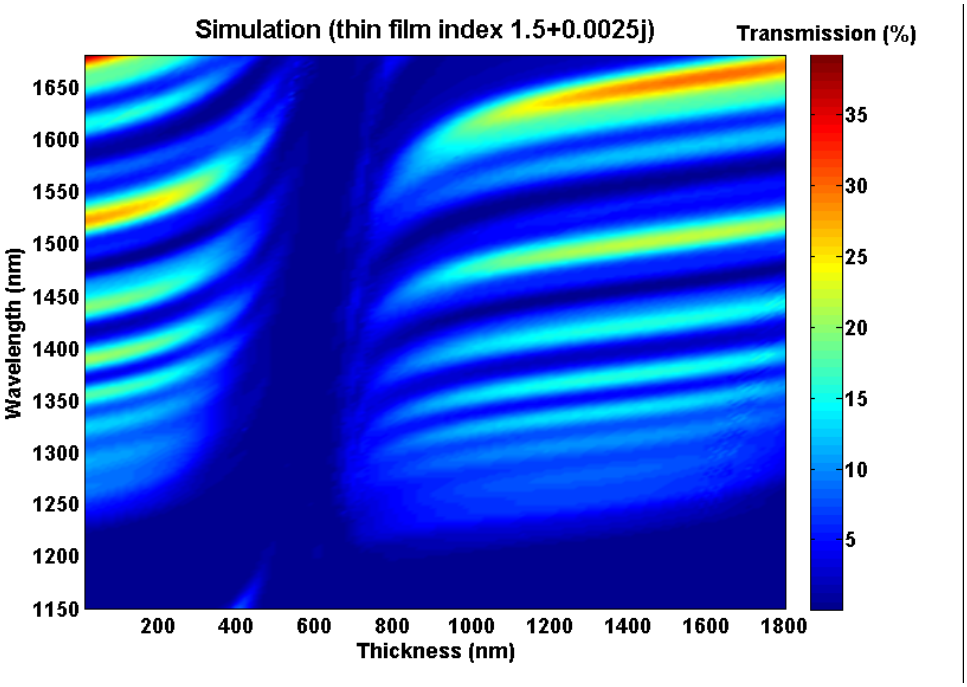

Fig. 12. Evolution of the spectrum as a function of thickness for an SMS structure of 20 mm (simulation with thin-film refractive index 1.5 + 0.0025i).

5. Conclusions

In this work it has been analyzed the evolution of the optical spectrum when depositing a thin-film of complex refractive index onto an SMS optical fiber structure for different no-core multimode segment lengths.

The presented results indicate three regions in the optical spectrum as a function of thin-film thickness. An initial region where transmission and attenuation bands shift to the red, a second region where these bands fade, and a third region where the bands reappear with some additional attenuation.

The numerical simulations obtained with the Transfer Matrix Method are corroborated with the experimental results, which permits to observe that the fading region occurs if the thin-film refractive index is complex. Otherwise, instead of a region where no transmission occurs, there is an abrupt modification of the bands.

By analyzing the evolution of the effective index of the modes and the coupling factor from the SMF core mode and the MMF modes it has been possible to understand why the bands outside de fading region experiment always a wavelength shift to the red instead of the wavelength shift to the blue observed in LPFGs. The reason is that in the SMS structure the difference between the effective indices of the modes is reduced as a function of the thin-film thickness, which causes a shift to higher wavelengths of the condition for constructive interference. However, in LPFGs the resonance wavelength is a function of the cladding effective index, which increases as a function of the thin-film thickness. This leads to a wavelength shift to the blue.

The main advantages of the SMS structure is its simplicity of fabrication (just two splices between a no-core fiber and two SMF pigtails), the possibility to monitor many bands in the optical spectrum, all of them experiencing a shift that is the same with the exception of a factor depending on the wavelength, and the possibility to reduce the size of the device without changing the sensitivity of the device.

#187483 - $15.00 USD Received 20 Mar 2013; revised 3 May 2013; accepted 13 May 2013; published 16 May 2013

The success obtained by earlier works in terms of development of applications such as chemical and biological sensors, refractometers, pH sensors and immunosensors, and the possibility studied in other works of increasing the sensitivity by reducing the core diameter, indicates that the structure studied in this work should become an interesting platform for the design of future sensors.

Acknowledgments

This work was supported by the Spanish Ministry of Education and Science-FEDER TEC2010-17805 and Government of Navarra research grants.

#187483 - $15.00 USD Received 20 Mar 2013; revised 3 May 2013; accepted 13 May 2013; published 16 May 2013